Carbon Deposition Assisting the Enhancement of Catalytic Activity with Time-on-Stream in the Dehydrogenation of Isobutane on NiO/Al_2O_3

Shigeru SUGIYAMA[1]*, Tashu YOSHIDA[1], Naohiro SHIMODA[1], Tomoyuki UEKI[2], Yuki KATO[3], and Wataru NINOMIYA[3]

[1]*Department of Applied Chemistry, Tokushima University, Minamijosanjima, Tokushima-shi, Tokushima 770-8506, Japan*

[2]*Graduate School of Technology, Industrial and Social Science, Tokushima University, Minamijosanjima, Tokushima-shi, Tokushima 770-8506, Japan 1*

[3]*Hiroshima R&D Center, Mitsubishi Chemical Corporation, 20-1, Miyuki-cho, Otake-shi, Hiroshima 739-0693, Japan*

Keywords: Dehydrogenation, Isobutane, Nickel Oxide, Catalyst Deactivation, Carbon Deposition

In the transformation reaction of alkanes to alkenes via catalytic dehydrogenation, it is generally accepted that the so-called catalytic deactivation behavior will occur. This phenomenon causes a drastic reduction in activity with time-on-stream. It is understood that carbon deposition generated during the reaction then covers the surface of the catalyst, and this leads to a drastic decrease in activity. However, contrary to this common wisdom, our laboratory reported that the dehydrogenation of isobutane to isobutene on $NiO/\gamma\text{-}Al_2O_3$ within a specific range of NiO loading in the presence of CO_2 actually improved the yield of isobutene with time-on-stream. Since few such cases have been reported, in this study, isobutane was dehydrogenated in the presence of CO_2 using $NiO/\alpha\text{-}Al_2O_3$ as the catalyst with 20% NiO loading and improvement was again observed. In order to investigate the cause of the improvement, both $NiO/\gamma\text{-}Al_2O_3$ and $NiO/\alpha\text{-}Al_2O_3$ with 20% NiO loading were examined in detail following the reaction. According to TEM analysis, both catalysts were covered with a large amount of carbon deposition after the reaction, but there was a difference in the types. The carbon deposition on $NiO/\gamma\text{-}Al_2O_3$ had a fibrous nature while that on $NiO/\alpha\text{-}Al_2O_3$ appeared to be a type of nanowire. Raman spectroscopy revealed that the carbonaceous crystal growth properties of two forms differed depending on the support. In particular, a catalytically active species of metallic nickel was formed in a high degree of dispersion in and on the above two forms of carbon deposition during the reaction, and this resulted in high activity even if the catalyst was covered with a carbon deposition.

Introduction

Researchers have accepted the inevitability of a heterogeneous catalytic reaction involving an organic chemical reaction on a solid catalyst, and that it will result in catalyst deactivation due to carbon deposition. In this case, carbon species derived from the reaction substrate are deposited on the catalyst surface during the catalytic reaction, and the catalytic active sites on the catalyst surface are covered with the carbon species, which drastically reduces catalytic activity with time-on-stream. Studies that attempt to prevent carbon deposition by using highly dispersed supported catalysts (Hayakawa *et al.*,1999; Takenaka *et al*., 2001; Takehira *et al*., 2002), or by doping basic oxides on the catalyst surface (Tomishige and Fujimoto, 1998; Razmgar *et al*., 2021), have often been reported. No studies, however, have shown that carbon deposition is not the cause of catalyst deactivation.

However, our group recently conducted the dehydrogenation of isobutane to isobutene on a $NiO/\gamma\text{-}Al_2O_3$ catalyst in the presence of CO_2 and found that the yield of isobutene was dramatically improved with time-on-stream despite remarkable amount of carbon deposition (Sugiyama *et al*., 2021). This result contradicts the opposite phenomenon to the conventional wisdom in this field. In other words, we suspected that carbon deposition, which is thought to be the main cause of catalyst deactivation, must have conversely contributed to an improvement in the catalytic activity. Furthermore, it is often pointed out that nanotube-like carbon deposition occurs around a Ni catalyst (Helveg *et al*., 2004; Abdi *et al*., 2006; Czaplicka *et al*., 2021). However, there have been no such observations concerning metallic nickel species, which is the active species for this reaction. Furthermore, it remains unknown whether this behavior is limited to $\gamma\text{-}Al_2O_3$ support.

In the present study, we investigated the dehydrogenation of isobutane to isobutene in the presence of CO_2 on $NiO/\alpha\text{-}Al_2O_3$ in order to elucidate these points. Furthermore, to clarify why the activity on both $NiO/\gamma\text{-}Al_2O_3$ and $NiO/\alpha\text{-}Al_2O_3$ was improved despite an excessive formation of carbon deposition, the state of carbon deposition and the catalytically active metallic nickel species were analyzed using a transmission electron microscope equipped with an energy-dispersive X-ray spectroscope. The study of coexistence of CO_2 in the present reaction system was reported by Ding *et al* (2010). The purpose for the

Received on March 28, 2022, Accepted on June 8, 2022

DOI:10.1252/jcej.22we031

Correspondence concerning this article should be addressed to S. Sugiyama (E-mail address: sugiyama@tokushima-u.ac.jp)

coexisting with CO_2 was to react with hydrogen obtained from dehydrogenation to produce water (reverse water gas shift reaction), followed by the successive reaction of water and carbon deposition to suppress carbon deposition. However, as was clear from our previous study (Sugiyama *et al*., 2021), it has been reported that significant carbon deposition progressed with or without the addition of CO_2.

1. Experimental Section

1.1 Preparation of the catalysts

The preparation procedures for both NiO/γ-Al_2O_3 and NiO/α-Al_2O_3 were essentially identical to that reported in previous papers (Ding *et al*., 2010; Sugiyama *et al*., 2021). NiO(20)/γ-Al_2O_3 and NiO(20)/α-Al_2O_3, in which "20" represents the weight % of NiO, was the focus in the present study, and the impregnation method used to prepare NiO(20)/α-Al_2O_3 is as follows. An aqueous solution (30 mL) was used to dissolve 3.984 g of $Ni(NO_3)_2{\cdot}6H_2O$ (Fujifilm Wako Pure Chemical Co.) and 4.000 g of α-Al_2O_3 (Fujifilm Wako Pure Chemical Co.). This suspension was evaporated to dryness at 383 K for 12 h. Finally, the resultant solid was calcined at 823 K.

1.2 Characterization of the catalysts

The nitrogen adsorption-desorption isotherms of the catalysts pretreated at 473 K for 5 h using a BELSORPmax12 (MicrotracBEL) at 77 K were used to calculate specific surface area, total pore volume, and average pore diameter. To obtain X-ray diffraction (XRD) patterns, we used a SmartLab/R/INP/DX (Rigaku Co.) equipped with a Cu Kα radiation monochromator at 45 kV and 150 mA. Thermogravimetric analysis (TGA) was investigated using an EXSTAR6000 (Seiko Instruments Inc.) under 100 mL/min of air flow with a heating rate of 8 K/min from 298-1073 K. Raman spectroscopy was measured using an inVia Reflex (Renishaw K. K.). Field emission scanning electron microscopy (FE-SEM) was recorded using a S-4700 (Hitachi High-Tech Corp.). A transmission electron microscope (JEM-2100F, JEOL) equipped with an energy dispersive X-ray spectroscope (SD60GV, JEOL) (EDS/TEM) was used for the analysis of the catalysts previously used for dehydrogenation.

1.3 Evaluation of catalytic performances

Activity testing was carried out using a fixed-bed continuous-flow reactor operated under atmospheric pressure at 823 K. A previously pelletized catalyst (0.25 g) was sieved to a size of 1.18–1.70 mm and loaded into the reactor. The temperature of the catalyst was increased to 823 K under a He flow at 11.0 mL/min. After the reaction temperature was stabilized, tests were carried out using a reactant gas that consisted of P(iso-C_4H_{10}) = 14.4 kPa, $P(CO_2)$ = 12.3 kPa, and P(He) = 74.6 kPa that was flowed into the reactor at a total flow rate of 15.0 mL/min. The homogeneous reactions were negligible under the present conditions. The reaction behavior was analyzed using a gas chromatograph (GC-8APT, Shimadzu Corp.) equipped with a thermal conductivity detector (TCD) and a capillary gas chromatograph (GC-2025, Shimadzu Corp.) equipped with a flame ionization detector (FID). The columns in the TCD-GC consisted of a molecular sieve (5A) (0.4 m × Φ 3 mm) for the detection of O_2, CH_4, and CO and a Porapak Q (6 m × Φ 3 mm) for the detection of CO_2, C_2H_4, C_2H_6, C_3H_6, and C_3H_8. An Rt-Alumina BOND/Na_2SO_4 (30 m × Φ 0.53 mm×10 μm) was used as a capillary column in the FID-GC to provide sufficient separation of iso-C_4H_{10} and iso-C_4H_8. The conversion and the selectivity were estimated on a carbon basis. The yield of isobutene was calculated from the product of the conversion of isobutane and the selectivity toward isobutene. Under the homogeneous reaction conditions in the absence of the catalysts, the conversions of iso-C_4H_{10} at 798 and 823 K were 0.0 and 0.8%, respectively. Therefore, there was almost no contribution of the homogeneous gas phase reaction.

2. Results and Discussions

2.1 Catalytic performances

The catalysts consisted of values of x that ranged from 18 to 23% in NiO(x)/γ-Al_2O_3 showed an evident enhancement in the yield of isobutene and the most evident enhancement was detected on NiO(20)/γ-Al_2O_3 (Sugiyama *et al*., 2021). Therefore, the catalysts with x = 20% became the focus. The dehydrogenations of isobutane at 823 K on NiO(20)/γ-Al_2O_3 and NiO(20)/α-Al_2O_3 are described in **Figures 1 (A)** and **(B)**, respectively. As shown in **Figure 1 (A)**, on NiO(20)/γ-Al_2O_3, the increase in isobutene yield with time-on-stream was reproduced as that in our previous paper (Sugiyama *et al.*, 2021). Similarly, the isobutene yield increased with time-on-stream on NiO(20)/α-Al_2O_3 (**Figure 1 (B)**). The conversions of CO_2 and isobutene yield on NiO(20)/γ-Al_2O_3 were greater than those on NiO(20)/α-Al_2O_3 probably due to greater levels of specific surface area, average pore diameter, and average pore diameter on NiO(20)/γ-Al_2O_3 than those on NiO(20)/α-Al_2O_3, as shown in **Table 1**. It is noteworthy that the conversion of isobutane on NiO(20)/α-Al_2O_3 was evidently greater than that on NiO(20)/γ-Al_2O_3 particularly till 2.0 h on-stream, indicating that the formation of carbon deposition had evidently proceeded on NiO(20)/α-Al_2O_3 particularly during the initial time-on-stream.

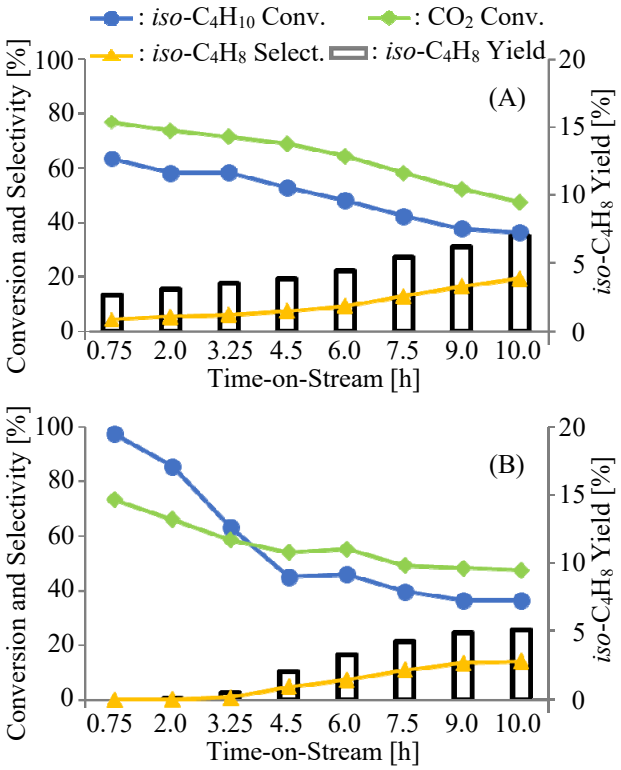

Fig. 1 The dehydrogenation of ethane at 823K on (A) NiO(20)/γ-Al_2O_3 and (B) NiO(20)/α-Al_2O_3

Table 1 Specific surface areas, total pore volumes, and average pore diameters of NiO(20)/γ-Al_2O_3 and NiO(20)/α-Al_2O_3

Support	Specific Surface area [m^2/g]	Total pore Volume [cm^3/g]	Average pore diameter [nm]
γ-Al_2O_3	156	0.519	13.3
α-Al_2O_3	8	0.089	36.1

It should be noted that the present results were derived from nickel-species and were largely unaffected by the support of γ-Al_2O_3 since the conversions of iso-C_4H_{10} at 0.75 and 6.0 h on-stream on γ-Al_2O_3 were 2.8 and 2.7% respectively.

2.2 Characterization of the catalysts before and after dehydrogenation using XRD and TGA

The XRD patterns of NiO(20)/γ-Al_2O_3 and NiO(20)/α-Al_2O_3 before and after the dehydrogenation of isobutane are shown in **Figure 2**. Prior to the dehydrogenation, the XRD peaks due to NiO (PDF 00-044-1159) and γ-Al_2O_3 (PDF 00-010-0425; Prins, 2020) from NiO(20)/γ-Al_2O_3 or NiO and α-Al_2O_3 (PDF 01-075-6776) from NiO(20)/α-Al_2O_3 were detected. After dehydrogenation, the XRD peaks due to Ni (PDF 00-004-0850), carbon (PDF 00-041-1487) and γ-Al_2O_3 from NiO(20)/γ-Al_2O_3 or Ni, carbon and α-Al_2O_3 from NiO(20)/α-Al_2O_3 were detected. It has been reported that NiO supported on γ-alumina was reduced using H_2 at the temperature lower than 673 K (Heracleous *et al.*, 2005). In addition, our laboratory also revealed that only metallic Ni signal was detected from the XRD of NiO(20)/γ-Al_2O_3 recovered at 0.1 h on-stream. Therefore, under the present reaction conditions, the reduction from NiO to Ni was completed promptly.

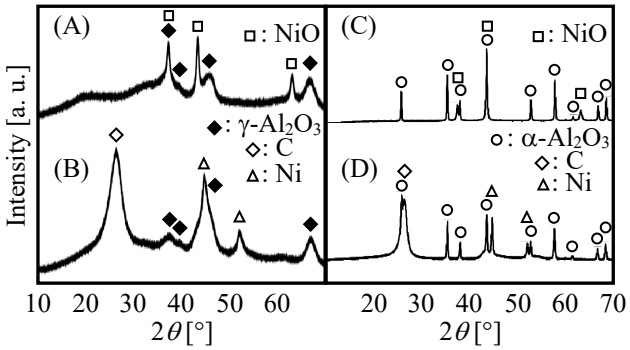

Fig. 2 XRD patterns of NiO(20)/γ-Al_2O_3 (A) before and (B) after dehydrogenation; and, the patterns of NiO(20)/α-Al_2O_3 (C) before and (D) after dehydrogenation

To quantify the amount of carbon deposition detected using XRD, TGA was used for both catalysts after the dehydrogenation of isobutane at 0.75, 6.0, and 10.0 on-stream. As shown in **Table 2**, the carbon deposition rate (CDR) per 1 g of catalyst increased with time-on-stream on both catalysts. For both catalysts, the rate of increase in CDR from 0.75 h to 6.0 h on-stream was evidently greater than that from 6.0 to 10.0 h on-stream. It should be noted that the CDR on NiO(20)/α-Al_2O_3 was evidently greater than that on NiO(20)/γ-Al_2O_3. The NiO particles formed on NiO(20)/α-Al_2O_3 would have been larger than those formed on NiO(20)/γ-Al_2O_3 due to the smaller specific surface area of NiO(20)/α-Al_2O_3 than that of NiO(20)/γ-Al_2O_3.

Table 2 Carbon deposition rate (CDR) for NiO(20)/γ-Al_2O_3 and NiO(20)/α-Al_2O_3 recovered after the dehydrogenation of isobutane at 0.75, 6.0, and 10.0 h on-stream

Catalyst	Time-on-stream [h]	CDR per 1 g of catalyst [g/g]
NiO(20)/γ-Al_2O_3	0.75	0.43
NiO(20)/γ-Al_2O_3	6.0	2.38
NiO(20)/γ-Al_2O_3	10.0	2.81
NiO(20)/α-Al_2O_3	0.75	0.80
NiO(20)/α-Al_2O_3	6.0	3.90
NiO(20)/α-Al_2O_3	10.0	4.91

Therefore, carbon deposition could have formed more easily on the metallic catalytic active species with a larger size, which has been reported using highly dispersed supported catalysts (Hayakawa *et al.*,1999; Takenaka *et al*., 2001; Takehira *et al*., 2002).

According to the results shown in **Figures 1** and **2**, the conversion of NiO to Ni and the formation of carbon deposition during dehydrogenation on both catalysts contributed to an increase in the isobutene yield with time-on-stream.

2.3 FE-SEM and EDS/TEM observations for carbon deposition and nickel species

Figure 3 shows FE-SEM images of (A) NiO(20)/γ-Al_2O_3 and (B) NiO(20)/α-Al_2O_3 after obtaining the results shown in **Figure 1** at 10.0 h on-stream.

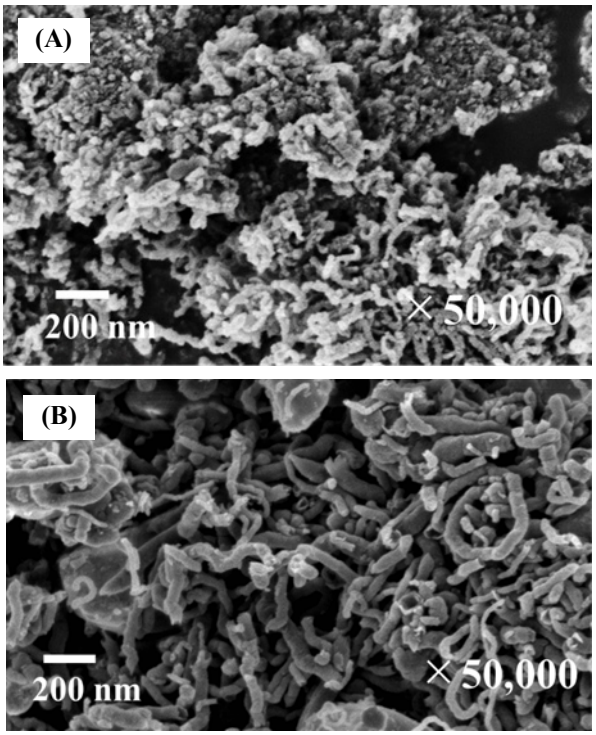

Fig. 3 FE-SEM images of (A) NiO(20)/γ-Al_2O_3 and (B) NiO(20)/α-Al_2O_3 after dehydrogenation at 10.0 h on-stream

A fine fibrous substance was detected from NiO(20)/γ-Al_2O_3. On the other hand, a fairly thick nanotube-type substance was detected on NiO(20)/α-Al_2O_3. If these substances are due to carbon deposition, this indicates a low degree of dispersion on NiO(20)/α-Al_2O_3, which is plausible due to the small specific surface area. On the other hand, carbon deposition likely formed with a high degree of dispersion on the larger specific surface area of NiO(20)/γ-Al_2O_3. Therefore, we suspect that fibrous substances with different thicknesses were formed based on the difference in the specific surface area of these catalysts.

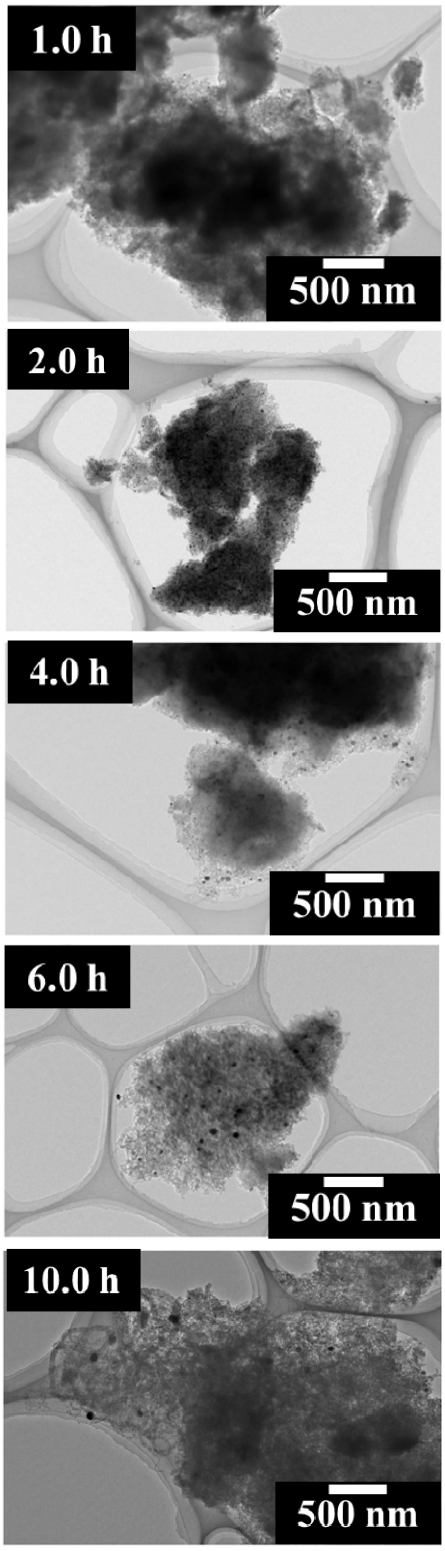

Fig. 4 TEM images of NiO(20)/γ-Al_2O_3 after the dehydrogenation at each time-on-stream

Both catalysts were analyzed by EDS/TEM to perform additional qualitative analysis of the substances

obtained by FE-SEM. **Figures 4** and **5** show the elapsed time for the states of carbon deposition with time-on-stream detected using TEM when NiO(20)/γ-Al_2O_3 and NiO(20)/α-Al_2O_3 were used for the activity test shown in **Figure 1**. These samples were obtained separately by repeating the experiments under the same conditions of the catalytic activity test to obtain the results shown **Figure 1**.

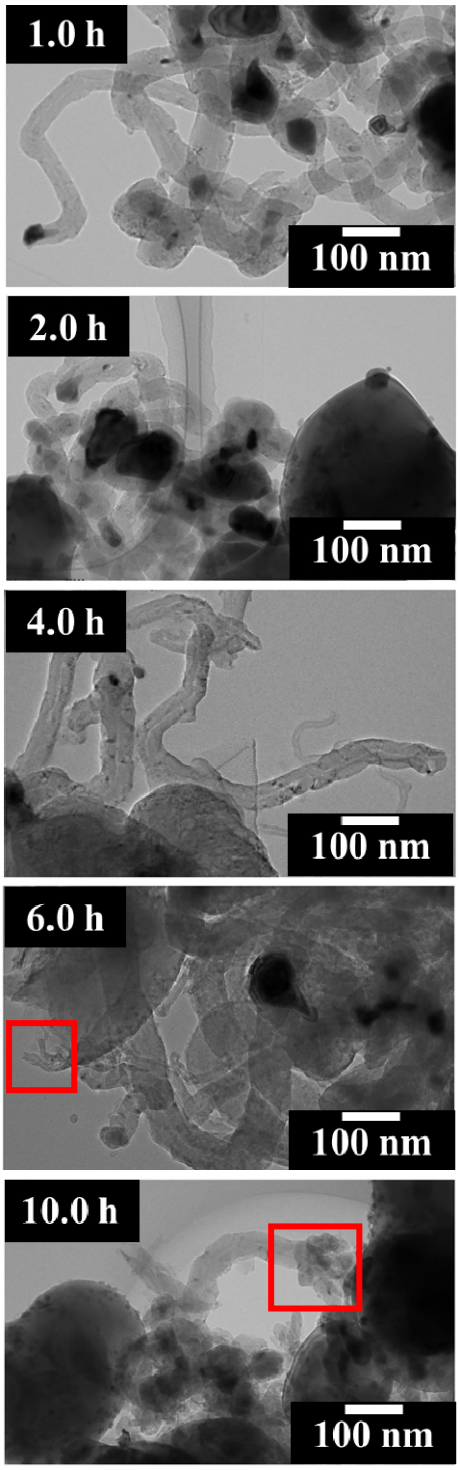

Fig. 5 TEM images of NiO(20)/α-Al_2O_3 following dehydrogenation at each level of time-on-stream

In the TEM images of NiO(20)/γ-Al_2O_3 following dehydrogenation (**Figure 4**), no apparent growth of a carbon nanotube-type substance was observed with time-on-stream. However, the growth of a hazy and fine fibrous substance was detected, particularly after 10 h on-stream. By contrast, in the TEM images of NiO(20)/α-Al_2O_3 following dehydrogenation (**Figure 5**), a carbon nanotube-type substance with a diameter of ca. 20 to 50 nm was detected on the catalyst even after a relatively short time of 1 h on-stream. There was a tendency for the diameter to increase with time-on-stream. Furthermore, after 6 and 10 h on-stream, we observed cracking at the tip of the carbon nanotube-type substance, which is highlighted in red in Figure 5.

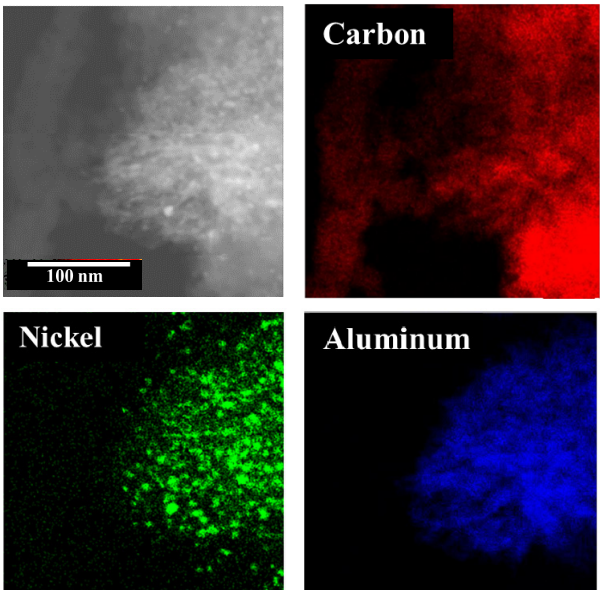

Fig. 6 EDS/TEM images of NiO(20)/γ-Al_2O_3 recovered at 6.0 h on-stream

We used EDS/TEM to determine the qualitative nature of the fibrous or carbon nanotube-type substances described above. **Figure 6** features the EDS/TEM images of NiO(20)/γ-Al_2O_3 recovered at 6.0 h on-stream. As shown in **Figure 6**, the hazy and fine fibrous substance in **Figure 4** was derived from carbon. Furthermore, metallic nickel (Nickel in **Figure 6**) particles with various particle size distributions were formed on alumina (Aluminum) and on the fibrous carbon (Carbon) with a high degree of dispersion. If nickel metal was formed with a high level of dispersion on the fibrous carbon deposited with time-on-stream, it is understandable that the yield of isobutene increased with time-on-stream, as shown in **Figure 1**.

As shown in **Figure 7**, the carbon nanotube-type substance detected from NiO(20)/α-Al_2O_3 **in Figure 5** was classified as carbon, based on the EDS/TEM image of NiO(20)/α-Al_2O_3 recovered at 10.0 h on-stream. This figure shows that a large amount of carbon nanotube-

type substance was deposited on the surface of the α-Al_2O_3 support because the signal due to aluminum could no longer be detected. From the signals due to metallic nickel, the metallic nickel could have been present both inside and on the surface of the carbon nanotube-type substance. In this case as well, since the metallic nickel particles had formed on the carbon nanotube-type substance with a high degree of dispersion with time-on-stream, this confirmed that the isobutene yield was improved with time-on-stream, as shown in Figure 1.

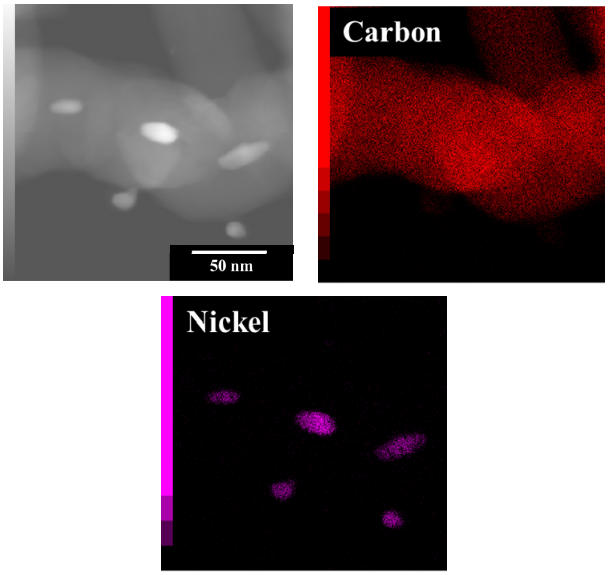

Fig. 7 EDS/TEM images of NiO(20)/α-Al_2O_3 recovered at 10.0 h on-stream

2.4 Employment of Raman spectroscopy for the observation of carbon deposition

As described above, a hazy and fine fibrous carbonaceous substance was formed from NiO(20)/γ-Al_2O_3, and a carbon nanotube-type substance was detected from NiO(20)/α-Al_2O_3. To clarify the characteristics of these carbonaceous substances, both catalysts were recovered at 0.75 h and 10 h on-stream and measured by Raman spectroscopy. When carbon nanotubes consisting of graphene (Iijima and Ichihashi, 1993) are analyzed by Raman spectroscopy, three types of signals are detected (Ferrari *et al*., 2006; Dresselhaus *et al*., 2010; Wang *et al*., 2019; Piao *et al*., 2021). The signal appearing around 2,700 cm^{-1} in the Raman shift was due to the crystallinity of graphite and is referred to as the G'-band. The signal appearing near 1,580 cm^{-1} is due to the planar structure of graphite and is referred to as the G-band, while that appearing around 1,350 cm^{-1} is due to the defective structure of graphite and is the D-band. A larger intensity for the G'-band signal and larger intensity ratios for the G-band and D-band signals (G/D ratio) translates to fewer defects in the carbon nanotubes (Ferrari *et al*., 2006; Dresselhaus *et al*., 2010; Wang *et al*., 2019; Piao *et al*., 2021). In the present study, a hazy and fine fibrous carbonaceous substance was formed from NiO(20)/γ-Al_2O_3, while a clear carbon nanotube-type substance was detected from NiO(20)/α-Al_2O_3. To clarify the characteristics of these carbonaceous substances following the reaction, the catalysts were measured by Raman spectroscopy.

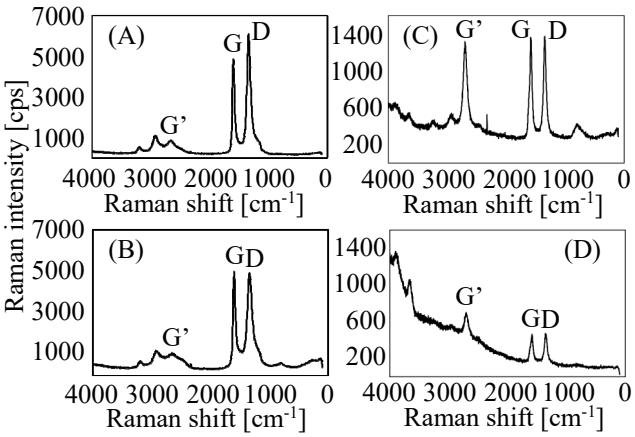

Fig. 8 Raman spectra of NiO(20)/γ-Al_2O_3 recovered at (A) 0.75 h and (B) 10.0 h on-stream together with NiO(20)/α-Al_2O_3 recovered at (C) 0.75 h and (D) 10.0 h on-stream

Figure 8 shows the Raman spectra of NiO(20)/γ-Al_2O_3 (**Figures 8 (A)** and **8 (B)**) and NiO(20)/α-Al_2O_3 (**Figures 8 (C)** and **8 (D)**) recovered after 0.75 h and 10.0 h, respectively. In the case of NiO(20)/γ-Al_2O_3, the intensity of the G'-band signal was extremely low. As shown in **Table 3**, the intensity of the G'-band and the G/D ratio increased with time-on-stream. That is, the carbonaceous substances in NiO(20)/γ-Al_2O_3 were formed gradually with time-on-stream, and the carbon nanotubes were formed with few defects. On the other hand, in the case of NiO(20)/α-Al_2O_3, three types of signals characteristic of carbon nanotubes were detected.

Table 3 G'-band intensity and G/D ratio obtained by Raman spectroscopy

Catalyst	Recovered time-on-stream [h]	G'-band intensity [cps]	G/D ratio [-]
NiO(20)/ γ-Al_2O_3	0.75	861	0.80
	10.0	1112	1.02
NiO(20)/ α-Al_2O_3	0.75	1304	0.99
	10.0	702	0.95

As shown in **Table 3**, the intensity of the G'-band and the G/D ratio decreased with time-on-stream. Therefore, in NiO(20)/α-Al_2O_3, the number of defective carbon nanotubes increases with time-on-stream. As shown in **Figure 5**, in NiO(20)/α-Al_2O_3, the tip of the

carbon nanotube-type substance cracked with time-on-stream, which is consistent with the present results obtained using Raman spectroscopy. As shown in **Figures 6** and **7**, the dispersed states of metallic nickel formed during the reaction in NiO(20)/γ-Al_2O_3 were evidently different from those in NiO(20)/α-Al_2O_3. This suggests that the dispersed state of nickel reflects the differences in the morphology of each carbon deposition detected in the Raman spectrum.

Conclusions

A hazy and fine fibrous carbonaceous substance was formed from NiO(20)/γ-Al_2O_3, while a clear carbon nanotube-type substance was detected from NiO(20)/α-Al_2O_3. The high dispersion of metallic nickel accompanying the formation of these carbonaceous substances contributed to the improvement in the isobutene yield with time-on-stream in the dehydrogenation of isobutane on those catalysts. When the amount of nickel oxide supported was small, even if high dispersion of metallic nickel occurred due to carbon deposition, the amount of the catalytic active species was so small that it was immediately covered with carbon deposition and exhibited normal deactivation behavior. Further, when the amount of nickel oxide supported was excessive, a large amount of carbon deposition covered the highly dispersed nickel metal as a catalytic active species. Therefore, the results of this study clarified that although there is a time-on-stream region and a nickel-loading region in which the isobutene yield was increased with time-on-stream, the dehydrogenation of isobutane was inactivated after a longer amount of time-on-stream.

Acknowledgements

This study was supported by JSPS KAKENHI Grant Number JP20K05221, for which we are grateful.

Literature Cited

Abdi, Y., J. Koohsorkhi, J. Derakhshandeh, S. Mohajerzadeh, H. Hoseinzadegan, M. D. Robertson, J. C. Bennett, X. Wu and H. Radamson; "PECVD-Grown Carbon Nanotubes on Silicon Substances with a Nickel-Seeded Tip-Growth Structure," *Mater. Sci. Eng. C*, **26**, 1219–1223 (2006)

Czaplicka, N., A. Rogala and I. Wyscocka; "Metal (Mo, W, Ti) Carbide Catalysts: Synthesis and Application as Alternative Catalysts for Dry Reforming of Hydrocarbons—A Review," *Int. J. Mol. Sci*., **22**, 12337 (2021)

Ding, J., R. Shao, J. Wu, Z. Qin and J. Wang; "Coupling Dehydrogenation of Isobutane to Produce Isobutene in Carbon Dioxide over NiO/γ-Al_2O_3 Catalyst," *React. Kinet. Mech. Catal*., **101**, 173–181 (2010)

Dresselhaus, M. S., A. Jorio, M. Hofmann, G. Dresselhaus and R. Saito; "Perspectives on Carbon Nanotubes and Graphene Raman Spectroscopy," *Nano. Lett.*, **10**, 751-758 (2010)

Ferrari, A. C., J. C. Meyer, V. Scardaci, C. Casiraghi, M. Lazzeri, F. Mauri, S. Piscanec, D. Jiang, K. S. Novoselov, S. Roth and A. K. Geim; "Raman Spectrum of Graphene and Graphene Layers," *Phys. Rev. Lett.*, **97**, 187401 (2006)

Hayakawa, T., S. Suzuki, J. Nakamura, T. Uchijima, S. Hamakawa, K. Suzuki, T. Shishido and K. Takehira; "CO_2 Reforming of CH_4 over Ni/Perovskite Catalysts Prepared by Solid Phase Crystallization Method," Appl. Catal. A. Gen., 183, 273-285 (1999)

Helveg, S., C. López-Cartes, J. Rehested, P. L. Hansen, B. S. Clausen, J. R. Rostrup-Nielsen, F. Abild-Pedersen and J. K. Nørskov; "Aromic-Scale Imaging of Carbon Nanofiber Growth," *Nature*, **427**, 426-429 (2004)

Heracleous, E., A. F. Lee, K. Wilson, and A. A. Lemonidou; "Investigation of Ni-Based Alumina-Supported Catalysts for the Oxidative Dehydrogenation of Ethane to Etylene: Structural Characterization and Reactivity Studies," *J. Catal*., **231**, 159-171 (2005)

Iijima, S. and T. Ichihashi; "Single-shell Carbon nanotubes of 1-nm diameter," *Nature*, **363**, 603-605

Piao, Y., V. N. Tondare, C. S. Davis, J. M. Gorham, E. J. Petersen, J. W. Gilman, K. Scott, A. E. Vladár and A. R. H. Walker; "Comparative Study of Multiwall Carbon Nanotube Nanocomposites by Raman, SEM, and XPS Measurement techniques," *Compos. Sci. Tech*., **208** 108753 (2021)

Prins, R.; "On the Structure of γ-Al_2O_3," *J. Catal*., **392**, 336-346 (2020)

Razmgar, K., M. Altarawneh, I. Oluwoye and G. Senanayake; "Ceria-Based Catalysts for Selective Hydrogenation Reactions: A Critical Review," Catal. Surv. Asia, 25, 27-47 (2021)

Sugiyama, S., K. Oribe, S. Endo, T. Yoshida, N. Shimoda, M. Katoh, Y. Kato, and W. Ninomiya; "Enhancement of the Catalytic Activity Associated with Carbon Deposition Formed on NiO/γ-Al_2O_3 Catalysts during the Direct Dehydrogenation of Isobutane," *J. Chem. Eng. Japan*, **54**, 35-43 (2021)

Takehira, K., T. Shishido and Kondo; "Partial Oxidation of CH_4 over Ni/$SrTiO_3$ Catalysts Prepared by a Solid-Phase Crystallization Method," *J. Catal*., **207**, 307-316 (2002)

Takenaka, S., H. Ogihara, I. Yamanaka and K. Otsuka; "Decomposition of Methane over Supported-Ni Catalysts: Effects of the Supports on the Catalytic Lifetime," *Appl. Catal., A. Gen.*, **217**, 101-110 (2001)

Tomishige, K. and K. Fujimoto; "Ultra-Stable Ni Catalysts for Methane Reforming by Carbon Dioxide," *Catal. Surv. Japan*, **2**, 3-15 (1998)

Wang, W., C. Wang, X. Yue, C. Zhang, C. Zhou, W. Wu and H. Zhu; "Raman Spectroscopy and Resistance-Temperature Studies of Functionalized Multiwalled Carbon Nanotubes/epoxy Resin Composite Film," *Microelect. Eng*., **214**, 50-54 (2019)